Scholars Journal of Physics, Mathematics and Statistics

OPEN ACCESS

Abbreviated Key Title: Sch J Phys Math Stat
ISSN 2393-8056 (Print) | ISSN 2393-8064 (Online)
Journal homepage: https://saspublishers.com

Structural Evolution of Rare-Earth Terbium Oxide Thin Films as Influenced by Growth Parameters and Post-Deposition Annealing Treatment

Abubakar A. Sifawa[1*], Iliyasu Usman[1], Anas Shehu[1]

[1]Department of Physics, Sokoto State University, Sokoto 852101, SSU, Sokoto, Nigeria

DOI: https://doi.org/10.36347/sjpms.2026.v13i01.002 | **Received:** 19.10.2025 | **Accepted:** 30.12.2025 | **Published:** 03.01.2026

***Corresponding author:** Abubakar A. Sifawa
Department of Physics, Sokoto State University, Sokoto 852101, SSU, Sokoto, Nigeria

1.1 Abstract

Original Research Article

Terbium oxide (Tb_4O^7) thin films were deposited on silicon (Si) substrates by radio frequency (RF) magnetron sputtering and subsequently subjected to low-temperature post-deposition annealing at 450 °C in an argon (Ar) atmosphere. Structural and surface analyses using grazing-incidence X-ray diffraction (GIXRD) and field emission scanning electron microscope equipped with energy dispersive X-ray (FESEM–EDX) revealed that annealing significantly enhanced the film crystallinity and surface morphology. The crystallite size increased from 14.06 nm to 24.58 nm, accompanied by a reduction in the lattice parameter toward the standard cubic Tb_4O_7 reference value. Clear grain growth and surface densification were observed after annealing. In addition, EDX analysis showed an increase in oxygen content, indicating a reduction in oxygen vacancy (V_o) concentration. These findings confirm that low-temperature Ar annealing is an effective approach for producing dense, uniform, and highly crystalline Tb_4O_7 thin films, making them suitable for silicon passivation and other low-thermal-budget semiconductor applications.

Keywords: Tb_4O_7 thin films; Crystallinity; GIXRD pattern; AFM roughness; annealing treatment; surface densification.

1.2 General Introduction

Thin films are essential to modern electronic devices, as they enable precise modification of surface properties at nanometer to micrometer scales [1,2]. These films are typically deposited on substrates to impart enhanced physical, chemical, and electronic functionalities. Si is the most widely used substrate in microelectronics due to its excellent electrical properties, mechanical stability, abundance, and cost-effectiveness, which make it ideal for large-scale semiconductor manufacturing [3,4]. Although alternative substrates such as GaAs, SiC, and sapphire are used in specialized applications, Si remains the dominant platform for integrated circuit fabrication [5].

The performance of thin films strongly depends on the deposition technique and process control. Various fabrication methods, including physical vapor deposition (PVD), chemical vapor deposition (CVD), atomic layer deposition (ALD), and sol–gel processing, have been widely employed [6–8]. Among these, radio-frequency (RF) magnetron sputtering is particularly suitable for oxide thin films, offering excellent control over film thickness, uniformity, stoichiometry, and adhesion at relatively low deposition temperatures [9].

Terbium oxide (Tb_4O_7) is a mixed-valence rare-earth oxide with properties favorable for semiconductor applications, including a wide bandgap (~2.23 eV), high refractive index, good optical transparency, and a relatively high dielectric constant [10,11]. In addition, Tb_4O_7 exhibits strong thermal and chemical stability, making it attractive for passivation and microelectronic device applications [12].

Post-deposition annealing (PDA) is commonly used to improve thin-film crystallinity and reduce defects [13]. Previous studies have shown that high-temperature annealing (600–900 °C) significantly enhances the properties of RF-sputtered Tb_4O_7 thin films on Si substrates

[9,14,15]. However, such conditions are not always suitable for applications that demand low thermal

budgets, such as flexible electronics, thin-film transistors (TFTs), and perovskite solar cells. This study presents a comparative analysis of as-sputtered Tb_4O_7 thin films and those subjected to PDA at 450 °C, focusing on their structural, morphological, topological, and optical characteristics. The films were deposited on Si substrates to evaluate their suitability for various applications in the semiconductor industry. The material was annealed for 20 min in an Ar atmosphere, and the study mainly focused on its physical properties.

2. Experimental Methods and Characterization

Si wafers were cleaned using the standard RCA process prior to film deposition. Organic contaminants were removed by immersing the substrates in an $H_2O/NH_4OH/H_2O_2$ (200:40:40 mL) solution at 75 °C for 10 min, followed by removal of the native oxide layer using a 1:50 HF/H_2O solution for 15 min. Metallic impurities were subsequently eliminated using an $H_2O/HCl/H_2O_2$ (240:40:40 mL) mixture at 75 °C for 10 min. The wafers were then thoroughly rinsed with deionized (DI) water and dried using nitrogen gas before deposition.

Structural characterization of the deposited thin films was carried out using grazing-incidence X-ray diffraction (GIXRD) with a Cu-Kα radiation source (λ = 1.5406 Å) on a Bruker D8 diffractometer. Surface morphology and elemental composition were examined using a field-emission scanning electron microscope (FESEM, FEI Nova NanoSEM 450) equipped with energy-dispersive X-ray spectroscopy (EDX).

3. RESULT AND DISCUSSION

3.1 Structural Studies

Fig. 1 presents the GIXRD patterns of both the as-sputtered film and the film annealed at 450 °C, deposited on a Si substrate. All diffraction peaks can be indexed to the cubic Tb_4O_7 phase (space group Fm-3m, 225), with preferred orientations along the (111), (200), (220), and (311) planes, particularly evident in the post-deposition annealed film, as confirmed by the International Centre for Diffraction Data (ICDD) database (file no. 00-013-0387). The diffraction features of the 450 °C annealed sample are consistent with earlier reports [10]. Both the as-sputtered and annealed films exhibit relatively crystalline characteristics. Notably, the as-sputtered film displayed only a dominant (111) orientation, while the peaks corresponding to the (200), (220), and (311) planes were poorly developed. Upon annealing, however, these orientations became well-defined, alongside the strong (111) peak. These results confirm that annealing not only enhances the crystallinity but also promotes the formation of multiple orientations in Tb_4O_7 thin films, a structural improvement that is critical for achieving high-performance and durable semiconductor device applications.

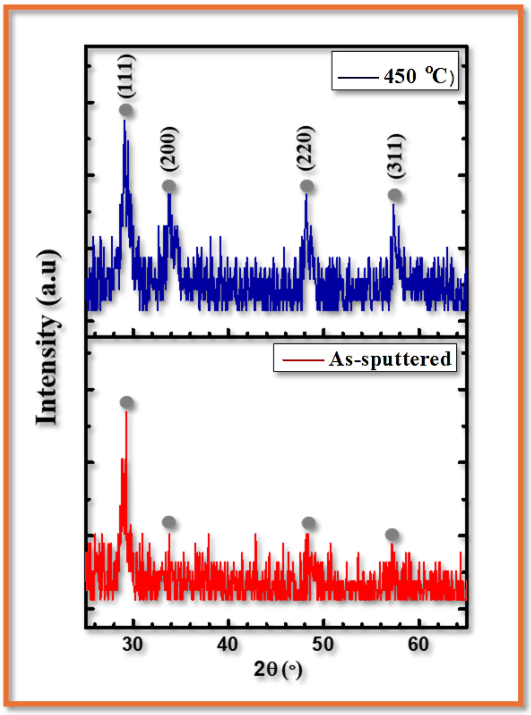

Figure 1. GIXRD pattern of the as-sputtered and annealed at 450 °C films

The Scherrer equation was utilized to evaluate the crystallite size (D) of the Tb_4O_7 thin films in order to gain deeper structural insights. The variation in D between the as-sputtered film and the sample annealed at 450 °C was calculated using equation (1) [16].

$$D = \frac{K\lambda}{\beta \cos\theta} \quad (1)$$

where D denotes the crystallite size, λ is the X-ray wavelength, and β represents the peak broadening along the 2θ axis, typically measured as the full width at half maximum (FWHM). θ corresponds to the Bragg angle, while K is the Scherrer constant, which varies between 0.62 and 2.08 depending on material morphology. In this work, a value of 0.9 was adopted for K.

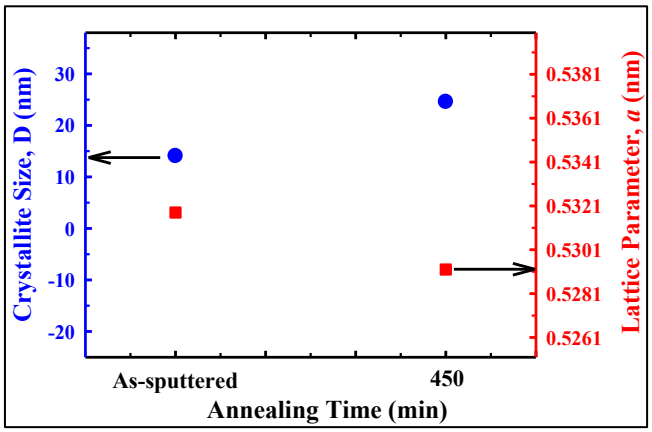

Figure 2. The Crystallite size and Lattice parameter for as-sputtered and annealed at 450 °C films

Figure 2 presents the calculated crystallite size (D) and lattice parameter (a) for the as-sputtered and 450 °C annealed Tb_4O_7 films. The as-sputtered film exhibits a D value of 14.06 nm, whereas the annealed film shows a markedly larger size of 24.58 nm, as shown in Table 1. This significant growth in crystallite size after post-deposition annealing can be attributed to thermally driven grain coalescence and the reduction of lattice defects, which facilitate crystal reordering and grain boundary migration [17].

In addition to crystallite size, the lattice parameter (a) for both the as-sputtered and 450 °C annealed films were determined from the position of the (111) diffraction peak using the cubic-system equations (2) and (3).

$$n\lambda = d_{hkl} \sin\theta \quad (2)$$

$$\frac{1}{d_{hkl^2}} = \frac{h^2 + k^2 + l^2}{a^2} \quad (3)$$

The lattice parameter (a) of the Tb_4O_7 films was determined from the (111) diffraction peak for both the as-sputtered and 450 °C annealed films. As shown in Figure 1, the peak position shifted slightly to a lower 2θ position from 29.056° for the as-sputtered film to 29.201° after annealing, yielding lattice parameters of 0.5318 nm and 0.5292 nm, respectively (see Table 1). These values are in excellent agreement with the cubic Tb_4O_7 reference pattern (a = .5290 nm) reported in the ICDD database, file no. 00-013-0387.

Table 1: Present the hkl values, angles, crystallite size, and lattice parameter

Annealing Temp. (ºC)	h k l	2θ (º)	FWHM β (2θº)	Crystallite size (nm)	Lattice parameter (nm)
As-sputtered	111	29.056	0.54671	14.06	0.5318
450	111	29.201	0.31267	24.58	0.5292

3.2 Surface Morphological studies

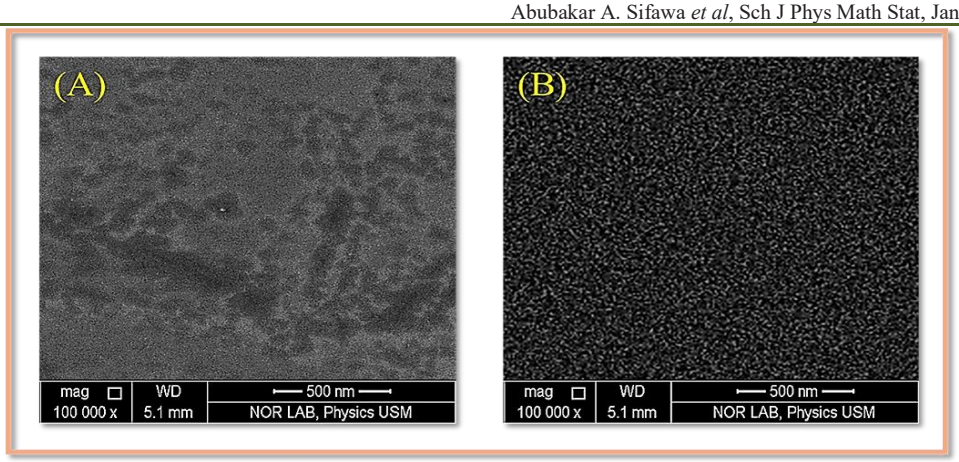

Figure 3: The top view FESEM images for as-sputtered and annealed at 450 °C films

Figure 3(A–B) shows the top-view FESEM images of the Tb_4O_7 films at 100,000× magnification, showing both the as-sputtered and annealed (450 °C) films. The as-sputtered film, as seen in Figure 3(A), features a morphology of extremely fine grains interspersed with notable voids. Following PDA at 450 °C, the surface appears smoother and nearly devoid of voids, with individual circular grains becoming indistinguishable (see Figure 3(B)). This transformation indicates thermally induced grain growth, wherein the expansion of adjacent grains merges to yield a larger average grain size and a denser film. The FESEM results are in good agreement with the crystallographic changes identified by the GIXRD analysis (Figure 1).

Figure 4(A and B) shows the EDX spectra of the Tb_4O_7 layers. The spectra reveal signals from Si, O, Tb, and a tiny amount of Ar, with the corresponding elemental ratios provided in the insets of Figure 4 (A and B) for both the as-deposited film and the film annealed at 450 °C. Intense Si peaks mainly originate from the underlying Si substrate rather than the deposition, while the Tb and O peaks align well with the expected film composition. A tiny Ar signal appears only after 450 °C annealing, attributable to the inert Ar environment and regarded as insignificant, with no additional elements observed. EDX further demonstrates a uniform spatial distribution of Tb, O, and Si, confirming strong interfacial bonding and even coverage of the Tb_4O_7 thin film across the Si surface.

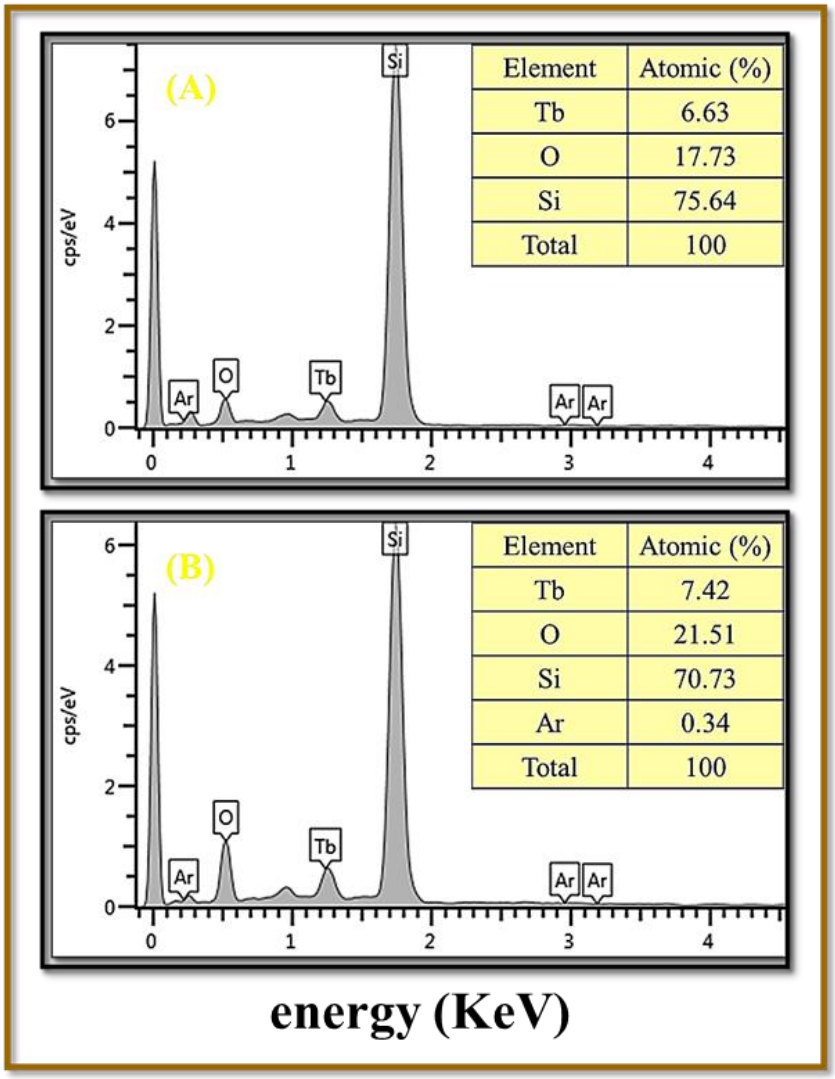

Figure 4(A and B): The EDX spectrum and elemental composition of as-sputtered and annealed at 450 °C films

The as-sputtered film contained a lower oxygen content (17.73 at. %) compared with the film annealed at 450 °C (21.51 at. %). During post-deposition annealing in Ar atmosphere, the supplied thermal energy promotes grain growth and helps eliminate oxygen vacancies (V_o). As a result, the lattice oxygen already present in the film becomes more evenly distributed, and the number of oxygen-deficient sites decreases, leading to a higher measured oxygen atomic percentage (at.%) even though no external O source is introduced [18].

4. CONCLUSION

Tb_4O_7 thin films deposited on Si by RF magnetron sputtering exhibit significant structural and morphological improvement after post-deposition annealing at 450 °C in an argon atmosphere. Annealing enhances crystallinity, promotes grain growth, reduces surface roughness, and increases oxygen stoichiometry, resulting in dense, smooth films suitable for low-thermal-budget and temperature-sensitive semiconductor applications.

Acknowledgement

We gratefully acknowledge the financial support provided by TETFund for the Institution Based Research (IBR) Grant No. TETF/DR&D/CE/UNIV/SOKOTO/IBR/2025/VOL.1, as well as the facilities and institutional support offered by Sokoto State University, which collectively fostered a conducive research environment and contributed to the successful outcome of this study.

REFERENCES

1. S. Yuvaraja, A. Nawaz, Q. Liu, D. Dubal, S. G. Surya, K. N. Salama and P. Sonar "Organic field-effect transistor-based flexible sensors," *Chem. Soc. Rev.*, vol. 49, no. 11, pp. 3423–3460, 2020, doi: 10.1039/c9cs00811j.
2. A. K. Katiyar, A. T. Hoang, D. Xu, J. Hong, B. J. Kim, S. Ji and J.H. Ahn, "2D Materials in Flexible Electronics: Recent Advances and Future Prospectives," *Chem. Rev.*, vol. 124, no. 2, pp. 318–419, 2024, doi: 10.1021/acs.chemrev.3c00302.
3. J. S. Park, M. Tang, S. Chen, and H. Liu,

"Heteroepitaxial growth of iii-v semiconductors on silicon," *Crystals*, vol. 10, no. 12, pp. 1–36, 2020, doi: 10.3390/cryst10121163.

4. X. Liu, C. Giordano, and M. Antonietti, "A molten-salt route for synthesis of Si and Ge nanoparticles: Chemical reduction of oxides by electrons solvated in salt melt," *J. Mater. Chem.*, vol. 22, no. 12, pp. 5454–5459, 2012, doi: 10.1039/c2jm15453f.
5. A. Elasser and T. P. Chow, "Silicon carbide benefits and advantages for power electronics circuits and systems," *Proc. IEEE*, vol. 90, no. 6, pp. 969–986, 2002, doi: 10.1109/JPROC.2002.1021562.
6. J. A. Oke and T. C. Jen, "Atomic layer deposition and other thin film deposition techniques: From principles to film properties," *J. Mater. Res. Technol.*, vol. 21, pp. 2481–2514, 2022, doi: 10.1016/j.jmrt.2022.10.064.
7. M. N. Chaudhari, "Thin film Deposition Methods: A Critical Review," *Int. J. Res. Appl. Sci. Eng. Technol.*, vol. 9, no. VI, pp. 5215–5232, 2021, doi: 10.22214/ijraset.2021.36154.
8. M. A. Butt, "Thin film Deposition Methods: A Critical Review. *International Journal for Research in Applied Science and Engineering Technology*, *9*(VI), 5215–5232. https://doi.org/10.22214/ijraset.2021.36154.
9. A. A. Sifawa, S. M. Mohammad, U. Iliyasu, M. Abdullah, Md. R. Shahrier, A. A. Soomro, and H. Naser, "The role of RF sputtering parameters on the uniformity and stability of Tb4O7 thin films on silicon substrates for passivation applications," *Phys. Scr.*, vol. 100, no. 2, p. 25910, 2025, doi: 10.1088/1402-4896/ada40a.
10. C. Zhu, C. Lv, M. Jiang, J. Zhou, D. Li, X. Ma, and D. Yang "Green electroluminescence from Tb_4O_7 films on silicon: Impact excitation of Tb^{3+} ions by hot carriers," *Appl. Phys. Lett.*, vol. 108, no. 5, 2016, doi: 10.1063/1.4941430.
11. S. V. Belaya, V. V. Bakovets, I. P. Asanov, I. V. Korolkov, and V. S. Sulyaeva, "MOCVD synthesis of terbium oxide films and their optical properties," *Chem. Vap. Depos.*, vol. 21, no. 4–6, pp. 150–155, 2015, doi: 10.1002/cvde.201507153.
12. B. M. Abu-Zied, A. R. N. Mohamed, and A. M. Asiri, "Effect of thermal treatment on the formation,textural and electrical conductivity properties of nanocrystalline Tb_4O_7," *J. Nanosci. Nanotechnol.*, vol. 15, no. 6, pp. 4487–4492, 2015, doi: 10.1166/jnn.2015.9605.
13. A. G. Khairnar and A. M. Mahajan, "Effect of post-deposition annealing temperature on RF-sputtered HfO_2 thin film for advanced CMOS technology," *Solid State Sci.*, vol. 15, pp. 24–28, 2013, doi: 10.1016/j.solidstatesciences.2012.09.010.
14. A. A. Sifawa, S. M. Mohammad, A. Muhammad, and W. F. Lim, "Influence of power and duration on RF sputtering for the formation of terbium oxide passivation layers via the argon ambient," *J. Mater. Sci. Mater. Electron.*, 2024, doi: 10.1007/s10854-024-12717-y.
15. A. A. Sifawa, S. M. Mohammad, A. Muhammad, S. M. Abed, and W. F. Lim, "The impact of post-deposition annealing durations on the formation of Tb_4O_7 passivation layer on silicon substrate," *Ceram. Int.*, vol. 50, no. 13PA, pp. 22430–22442, 2024, doi: 10.1016/j.ceramint.2024.03.344.
16. R. Shahrier, S. M. Mohammad, and M. Abdullah, "Annealing - driven third - order optical nonlinear properties of naturally oxidized copper oxide thin films," 2025.
17. M. H. Majeed, M. Aycibin, A. G. Imer, A. M. Muhammad, and M. M. Kareem, "Influence of annealing process on structural, optical and electronic properties of nano-structured ZnO films synthesized by hydrothermal technique: Supported by DFT study," *Mater. Sci. Eng. B*, vol. 282, no. May, p. 115793, 2022, doi: 10.1016/j.mseb.2022.115793.
18. X. Y. Zhang, J. Han, Y. T. Wang, Y. J. Ruan, W. Y. Wu, D. S. Wuu, J. Zuo, F. M. Lai, S. Y. Lien, W. Z. Zhu**,** "Effect on passivation mechanism and properties of HfO2/crystalline-Si interface under different annealing atmosphere," *Sol. Energy Mater. Sol. Cells*, vol. 257, no. May, p. 112384, 2023, doi: 10.1016/j.solmat.2023.112384.